Research article

Bulk and single-cell RNA sequencing reveal the contribution of laminin γ2 -CD44 to the immune resistance in lymphocyte-infiltrated squamous lung cancer subtype

Tingting Song , Ying Yang , Yilong Wang , Yinyun Ni , Yongfeng Yang [*], Li Zhang [**]

Institute of Respiratory Health, Frontiers Science Center for Disease-related Molecular Network, State Key Laboratory of Respiratory Health and Multimorbidity, West China Hospital, Sichuan University, Chengdu, 610041, China

ABSTRACT

The high heterogeneity of lung squamous cell carcinomas (LUSC) and the complex tumor microenvironment lead to non-response to immunotherapy in many patients. Therefore, characterizing the heterogeneity of the tumor microenvironment in patients with LUSC and further exploring the immune features and molecular mechanisms that lead to immune resistance will help improve the efficacy of immunotherapy in such patients. Herein, we retrospectively analyzed the RNA sequencing (RNA-seq) data of 513 LUSC samples with other multiomics and single-cell RNA-seq data and validated key features using multiplex immunohistochemistry. We divided these samples into six subtypes (CS1–CS6) based on the RNA-seq data and found that CS3 activates the immune response with a high level of lymphocyte infiltration and gathers a large number of patients with advanced-stage disease but increases the expression of exhausted markers cytotoxic T-lymphocyte associated protein 4, lymphocyte-activation gene 3, and programmed death-1. The prediction of the response to immunotherapy showed that CS3 is potentially resistant to immune checkpoint blockade therapy, and multi-omic data analysis revealed that CS3 specifically expresses immunosuppression-related proteins B cell lymphoma 2, GRB2-associated binding protein, and dual-specificity phosphatase 4 and has a high mutation ratio of the driver gene ATP binding cassette subfamily A member 13. Furthermore, single-cell RNA-seq verified lymphocyte infiltration in the CS3 subtype and revealed a positive relationship between the expression of LAMC2-CD44 and immune resistance. LAMC2 and CD44 are epithelial-mesenchymal transition-associated genes that modulate tumor proliferation, and multicolor immunofluorescence validated the negative relationship between the expression of LAMC2-CD44 and immune infiltration. Thus, we identified a lymphocyte-infiltrated subtype (CS3) in patients with LUSC that exhibited resistance to immune checkpoint blockade therapy, and the co-hyperexpression of LAMC2-CD44 contributed to immune resistance, which could potentially improve immunological efficacy by targeting this molecule pair in combination with immunotherapy.

* Corresponding author. Department of Respiratory and Critical Care Medicine, West China Hospital of Sichuan University Chengdu, 610041, China.
** Corresponding author.
E-mail addresses: yangyongfeng0523@163.com (Y. Yang), zhangli2809@wchscu.cn (L. Zhang).

Abbreviations

LUSC	squamous cell lung cancer
LUAD	lung adenocarcinomas
NSCLC	non-small cell lung cancer
ICB	Immune Checkpoint Blockade
TIBs	tumor-infiltrating B lymphocytes
TME	tumor microevnironment
EMT	epithelial-mesenchymal transition
scRNA-seq	single-cell RNA sequencing
mIHC	Multiplex immunohistochemical
TCGA	the Cancer Genome Atlas
CS	consensus subtype
miRNA	microRNA
mRNA	master RNA
lncRNA	long non-coding RNA
CIBERSORT	Cell-type Identification By Estimating Relative Subsets Of RNA Transcripts
ESTIMATE	Estimation of STromal and Immune cells in MAlignant Tumor tissues using Expression data
TIDE	Tumor Immune Dysfunction and Exclusion
TMB	Tumor mutation berdon
ssGSEA	single sample gene set enrichment analysis
FGA	fraction of genome altered
FGL	fraction of genome lost
FGG	fraction of genome gained

1. Introduction

Lung squamous cell carcinoma (squamous cell lung cancer [LUSC]) is a high-mortality cancer with limited treatment options and accounts for 20%–30 % of non-small cell lung cancer (NSCLC), which is the leading cause of cancer-related deaths worldwide [1,2]. Its pathological features are marked squamous differentiation, and C/K56 is a commonly used immunohistochemical marker. Unlike lung adenocarcinomas (LUAD), patients with LUSC do not benefit from targeted therapies because common driver mutations found in LUAD are rarely identified, and efforts to identify driver mutations in LUSC have not been fruitful [3–6]. The advent of immuno-therapies such as immune checkpoint blockade (ICB) therapy, which can destroy tumor cells by reactivating immune cells and relieving the inhibitory effects of these immune cells due to their production of inhibitors, has revolutionized clinical management and has been a successful therapeutic strategy for patients with LUSC [7–11]. Owing to the high individual heterogeneity of patients with LUSC, especially those in advanced stages, some patients with high immune checkpoint expression do not respond to ICB therapy. Thus, more effective treatments are urgently needed, which can be developed based on a comprehensive knowledge of the genetic factors for LUSC.

The tumor microenvironment develops and evolves through the interplay between tumor cells and various immune and non-immune stromal cells [12], and the composition of the tumor microenvironment has been shown to influence the response to ICB therapy [13]. For instance, increased infiltration of CD8$^+$ T cells leads to a good response to ICB therapy [14–16]. The tumor-infiltrating B lymphocytes play an anti-tumor immunity role in lung cancer [17–20]. Plasma cells have been reported as prognostic markers for programmed death-ligand 1 (PD-L1) immunotherapy in NSCLC patients [21]. However, the infiltration of CD36$^+$CD8+T cells determines the exhausted tumor microenvironment in NSCLC patients, with a positive correlation with immu-nosuppressive cells Tregs and M2-polarized macrophages as well as programmed death-1 (PD-1) and T cell immunoreceptor with Ig and ITIM domains (TIGIT) [22]. Tumor-associated macrophages suppress adaptive immune responses by increasing the expression of immune checkpoint molecules (PD-L1, PD-L2, and B7–H4), resulting in T cell exhaustion [23–25]. Furthermore, exhausted T cells, which express PD-L1, hepatitis A virus cellular receptor 2 (HAVCR2), cytotoxic T-lymphocyte associated protein 4 (CTLA4), lymphocyte-activation gene 3 (LAG3), TIGIT, etc., in tumors, gain suppressor activity and can restrain immunity, especially terminally exhausted T cells [26–28].

In addition, cell communication based on signaling molecular is an important driver of tumour development, such as interleukins [29], which is associated with a wide range of diseases and disorders, and toll-like resceptors [30], which modulates the human immune responses at innate as well as adaptive levels and as suitable targets for developing immunotherapeutics against cancer. CD44 is a common biomarker of cancer stem cells and is involved in the epithelial-mesenchymal transition (EMT) and modulation of cancer proliferation, invasion, metastasis, and therapy resistance [31]. High levels of CD44 are negatively correlated with lymphatic invasion in colorectal tumors [32]. Laminin γ2 (LAMC2) is an EMT-associated gene. Its high expression can promote invasion, migration, and metastasis in LUAD [33] and promote macrophage infiltration and extracellular matrix remodeling in NSCLC [34]. However, few studies have focused on the influence of co-expression and molecular communication of LAMC2-CD44 on LUSC.

Single-cell RNA sequencing (scRNA-seq) technology is a powerful tool for dissecting the tumor microenvironment, which allows

the study of heterogeneity between different phenotypes, cell types, and functional states at the single-cell level [35]. Multiplex immunohistochemistry (mIHC) is a novel immunochemical technique that can detect multiple targets in tissue samples to comprehensively study cellular composition, function, and biomarker expression [36–38]. Thus, characterizing the tumor microenvironment of LUSC and exploring the genetic and molecular characteristics of different tumor phenotypes using bulk and scRNA-seq data, along with mIHC, can help uncover immune resistance mechanisms and provide new ideas for tumor treatment.

In this study, we divided 513 LUSC samples from The Cancer Genome Atlas (TCGA) into six consensus subtypes (CS1–CS6) according to transcriptomic expression and demonstrated that subtype 3 (CS3) is a lymphocyte-infiltrated tumor subtype, with high expression of exhausted markers and resistance to ICB therapy. We further found that LAMC2-CD44 plays an important role in the immune resistance of the CS3 subtype.

2. Material and methods

2.1. Datasets

Bulk multiomic data download: We downloaded the RNA, microRNA (miRNA), copy number alternatio, single nucleotide polymorphism (SNP) datasets, and clinical information of LUSC from the TCGA database (https://www.genome.gov). We also downloaded the protein data of LUSC samples from the National Cancer Institute's Clinical Proteomic Tumor Analysis Consortium TCGA-LUSC cohort. Furthermore, we obtained one RNA-seq validation dataset and protein data from a public study on LUSC [39] (transcriptomic data files can be accessed at the Genomic Data Commons; https://portal.gdc.cancer.gov/, via dbGaP Study Accession: phs001287.v10.p5). We also obtained two immunotherapy cohorts: urothelial carcinoma (BLCA) from the IMvigor210CoreBiologies R package (version 1.0.0) [40] and 51 NSCLC samples from the GEO database (https://www.ncbi.nlm.nih.gov/geo/) via GSE207422 and GSE135222.

ScRNA-seq data: The scRNA-seq data of LUSC from a previously published study [41] by our research group contained eight paired patients with primary and adjacent LUSC in 16 squamous carcinoma samples.

2.2. RNA-seq data analyses

Sample subtyping: For the RNA-seq and miRNA-seq data from the TCGA database, 513 LUSC samples were retained for further analysis, and the RNA-seq data were divided into mRNA and long non-coding RNA (lncRNA) according to the gene annotation file from the Ensembl database (gencode.v27.long_noncoding_RNAs.gtf). We also identified the genes that were expressed in more than half of the samples and ranked them in the top 75 % by the standard deviation values in all samples. We then applied the getMOIC function from the MOVICS package (version 0.99.17) [42] and subtyped these 513 LUSC samples into six subtypes (CS1–CS6) based on RNA and miRNA-seq data using iClusterBayes, SNF, PINSPlus, NEMO, COCA, LRAcluster, ConsensusClustering, IntNMF, CIMLR, MoCluster algorithms, and Euclidean distance. The silhouette coefficient was used to depict how well the data points fit the clusters to which they were assigned.

Survival analyses of subtypes To estimate the prognostic difference among these identified subtypes, we used the compSurv function from the MOVICS package to calculate the Kaplan–Meier estimator and generated survival curves with the log-rank test to detect prognostic differences by pair-wise comparisons.

Function annotation: We identified the feature markers for each subtype using the runMarker function from the MOVICS package with the edgeR method and filtered by the p-value and false discovery rate≤0.05. We performed gene set variation analysis (GSVA) for each subgroup using the runGSEA function from the MOVICS package with the cutoff of p-value set as 0.05 and false discovery rate set as 0.25. We further applied the functional annotation of each subtype using the Metascape database (https://metascape.org/gp/index.html) based on the top 400 genes; the p-value was set as 0.01, and Min Enrichment was set as 1.5. Finally, we downloaded 16 immune-related gene sets from the ImmPort database and calculated their enrichment scores in each sample using the ssGSEA function from the GSVA package (version 1.44.2) with the tau value set to 0.25.

Validation of the test dataset: To further validate the subtypes of LUSC samples from the TCGA database, we downloaded the RNA-seq data of 108 patients with LUSC, including 108 tumors and 94 adjacent tumor samples, from a public study [39] and applied the same filtering process of RNA-seq data from TCGA-LUSC. We then used the runNTP function from the MOVICS package to characterize these samples using the same cluster biomarkers obtained using the runMarker function of TCGA-LUSC subtypes. Additionally, we annotated these new subtypes in 202 samples using well-defined tumor types in this published study.

Immune feature characterization of each subtype: CIBERSORT (Cell-type Identification By Estimating Relative Subsets Of RNA Transcripts) (version 0.1.0) [43] was used to estimate the degree and proportion of 22 types of immune cell infiltration for each subtype, based on a linear support vector regression. ESTIMATE (Estimation of STromal and Immune cells in MAlignant Tumor tissues using Expression data) (version 1.0.13) [44] was used to calculate the immune and stromal scores. Nine immune-active markers, six immune checkpoint markers, and 14 B cell markers were also evaluated between the subtypes (Supplementary Table 2). We further predicted the enrichment score of 2181 immune-related genes obtained from the Immunology Database and Analysis Portal (ImmPort) (https://immport.niaid.nih.gov) using single-sample gene set enrichment analysis (ssGSEA).

2.3. scRNA-seq data analyses

Cell clustering and annotation: We used published scRNA-seq data from eight LUSC tumors and adjacent normal tissues. The matrix

of read counts per gene per sample was further analyzed using the Seurat package (version 4.1.1) in the R software (version 4.2.0). Cells meeting any of the following criteria were excluded: (1) <200 and >2500 expressed genes, (2) > 5 % unique molecular indices of mitochondrial genes, (3) <80 % cell complexes, which were calculated using the nFeature_RNA/nCount_RNA. The gene expression matrix of each sample was normalized using the NormalizeData function with default parameters, and 2000 variable features were found using the FindVariableFeatures function. The standard anchor-based workflow for dataset integration in Seurat was used to adjust for the biological sources of variation between samples. Principal component analysis was performed, and the first 13 principal components (PCs) were used in the FindNeighbor function. The resolution parameter of the FindClusters function was set to 0.5. Uniform manifold approximation and projection was performed for visualization in two dimensions using the RunUMAP function with the same PCs and other default parameters. The marker genes for each cluster were found using the FindAllMarkers function with the parameter "min.pct = 0.25, thresh.use = 0.25." Finally, we grouped these cells into 37 clusters and annotated them using well-known classical markers. Cell types were validated using the SingleR package. The enrichment scores of tumor-infiltrating B lymphocyte-related genes from published reviews were scored using the AddModuleScore function in the Seurat package.

Phenotype annotation of single-cell data (Scissor analysis): To explore the cell composition of specific subtypes of LUSC, we used the scissor R package (version 2.1.0) [45], which can predict enriched cells of a defined tumor type by combining single-cell and bulk data. First, we annotated the 513 samples as CS3 and Rest groups, then performed the Scissor function on dates of bulk RNA-seq and scRNA-seq with the parameter "alpha = 0.01, cutoff = 0.03, family = binomial."

Sub-clustering the scissor-predicted cells: The cells that were enriched in the CS3 and Rest groups predicted by the scissor package were selected and subjected to sub-clustering analysis with the first 12 PCs used in the FindNeighbors function, and 0.5 resolution was used in the FindClusters function. The RunUMAP and FindAllMarker functions use the same parameters described above. These cells were sub-clustered into 17 clusters and annotated using classical markers.

Cell-cell communication: We used the Cellchat package (version 1.5.0) with default parameters to detect the differential communication of cell types between CS3 and Rest using the single-cell gene expression matrix and the ligand-receptor information contained in the package, which modeled the communication probability and identified significant communications. The communication molecular pairs between cells in the two groups were predicted by the computeCommunProb function with default parameters, and the signaling pathways were predicted by the computeCommunProbPathway function with default parameters. To identify functional pathway change, we also delineated signaling changes between CS3 and Rest using the computeNetSimilarityPairwise function.

2.4. Clinical data analyses

For the clinical data of these samples, we selected the sex, prior malignancy, stage, smoking history, age, and new tumor event information and calculated a 95 % confidence interval p-value by Cox analysis to evaluate the difference between the subtypes. The results were visualized using a forest plot.

2.5. Genome data analyses [46]

For genomic data, we downloaded the copy number variation and SNP (simple nucleotide variation) dates of LUSC from the TCGA database and obtained 513 samples, which matched the RNA-seq data. We then computed the fraction of genome altered (FGA), fraction of genome lost (FGL), and fraction of genome gained (FGG) using the copy number variation data using the compFGA function from the MOVICS package (version 0.99.17), with the default parameters in R [42]. For SNP data, we visualized the top mutated genes using the oncoplot function from the maftools package (version 2.12.0) and calculated the co-occurring events between the selected genes using the somaticInteractions function from the maftools package in each subtype. We also obtained tumor mutation burden (TMB) data for each sample using the tmb function of the maftools package, and the difference between subtypes for TMB was evaluated using the Wilcoxon test.

2.6. Prediction module and therapy response for CS3

For the CS3 subtype, we developed a prediction module using the randomForest package (version 4.7–1.1). The 513 samples were divided into training and test data in a 3:1 ratio, and the Boruta algorithm from the Boruta package (version 8.0.0) was used to select important factors based on CS3-specific marker genes. To evaluate the immunotherapy response, we predicted the ICB therapy response of all tumor samples based on the tumor immune dysfunction and exclusion (TIDE) (TIDE value, which was calculated using the TIDE algorithm on the website (TIDE (Harvard. edu)), the cancer type parameter set as NSCLC, and the previous immunotherapy set as NO [47]. The same TIDE analysis was applied to the validation dataset (202 samples). We then performed a different analysis between CS3 and the other tumor subtypes (CS1, CS2, CS5, and CS6) based on the TIDE value. For the immunotherapy cohort data of urothelial carcinoma (BLCA) and 51 NSCLC, we first calculated the enrichment score for the predictive factors of CS3 using the ssGSEA analysis and then performed different analyses between complete response/partial response (CR/PR) and progressive disease/stable disease (PD/SD) groups based on them.

2.7. Opal Multiplex immunohistochemistry, mIHC

In this study, we used The Opal Polaris 7-color Manual IHC Kit to perform mIHC 4-μm sections of clinical paraffin tissue from 4 patients with LUSC, with the consent of patients and the approval of the Department of Pathology, West China Hospital (Table S3).

These four patients with LUSC were all male smokers, with an age distribution of 59–76, and contained pathological stages I–III. The primary difference between the two is the degree of differentiation. Before performing mIHC, the sections were dewaxed and rehydrated using xylene and a gradient alcohol solution, and the concentrations of antibodies were determined using conventional IHC. For the mIHC experiment, one tissue sample was stained with five antibodies: CD3 (Abcam, ab16669), CD19 (Abcam, ab134114), CD44 (Affinity, DF6392), LAMC2 (Abcam, ab210959), and CK5/6 (Millipore, MAB1620). Five incubations with the primary antibody,
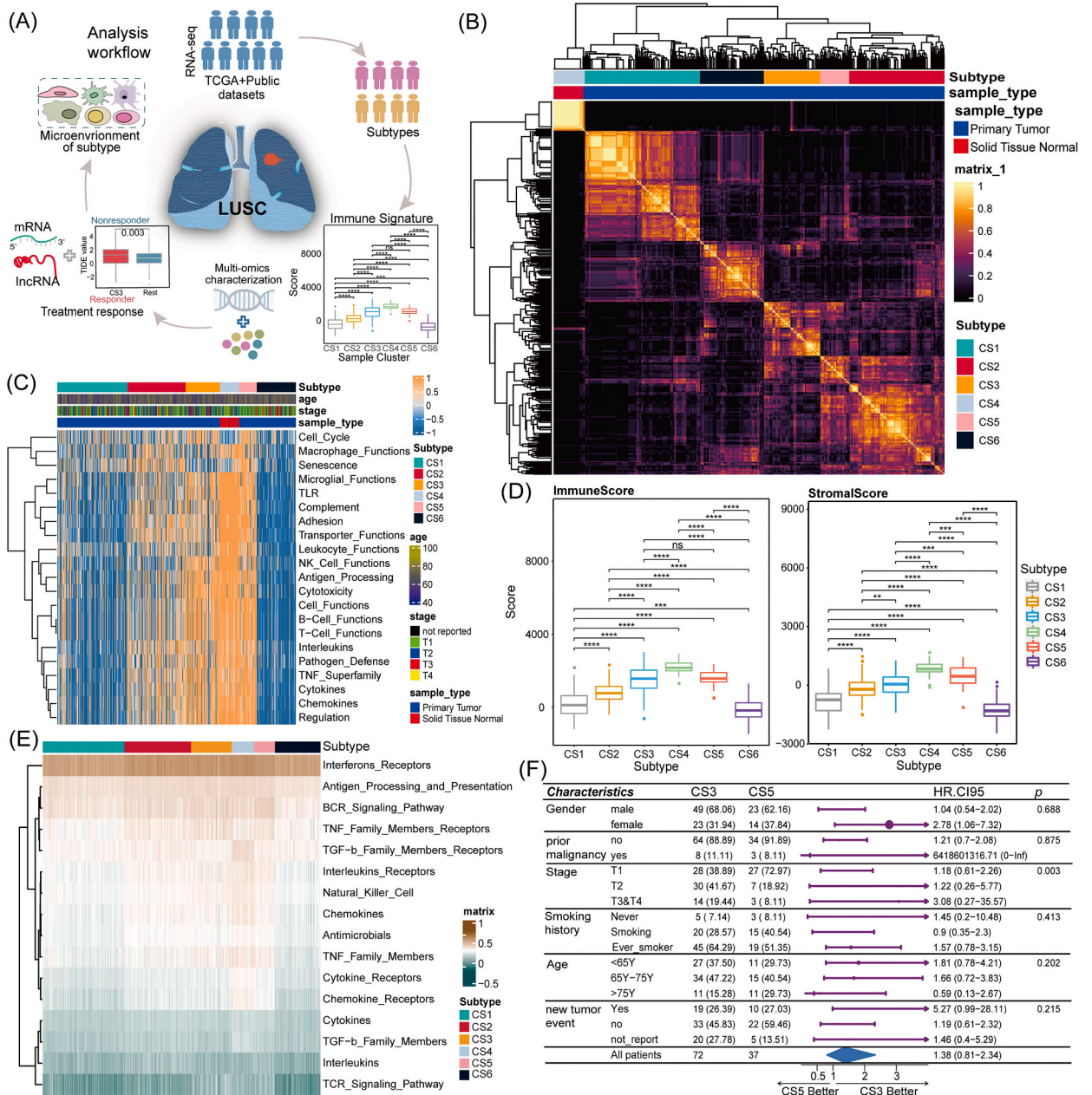

Fig. 1. Identification of sub-types for LUSC patients based on the bulk RNA-seq data. (A) Schematic showing the analysis workflow of TCGA-LUSC RNA-seq profiling and the various data types generated in this study. (B) Consenses heatmap indicating the consistency of the samples in the six identified subtypes and using the euclidean method to calculate the distance between any two subtype. These samples were annotated by sample_type. (C) GSVA analysis calculated the pathways enrichment score for single samples in this study, and annotated by age, Subtype, stage and sample_type. (D) Boxplot showing the distribution of ImmuneScore and StromalScore for each sub-type calculated by ESTIMATE (Estimation of STromal and Immune cells in MAlignant Tumour tissues using Expression data). The P value was calculated by wilcox.test. ****: $P < 0.0001$, ***: $0.0001 \leq P < 0.001$, **: $0.001 \leq P < 0.01$, *: $0.01 \leq P < 0.05$. (E) Heatmap showing the enrichment score of 16 immune-related gene sets from ImmPort database in each samples, which was calculated by the ssGSEA algorithm. (F) Forestplot indicating the clinical information differences between CS5 versus CS3.
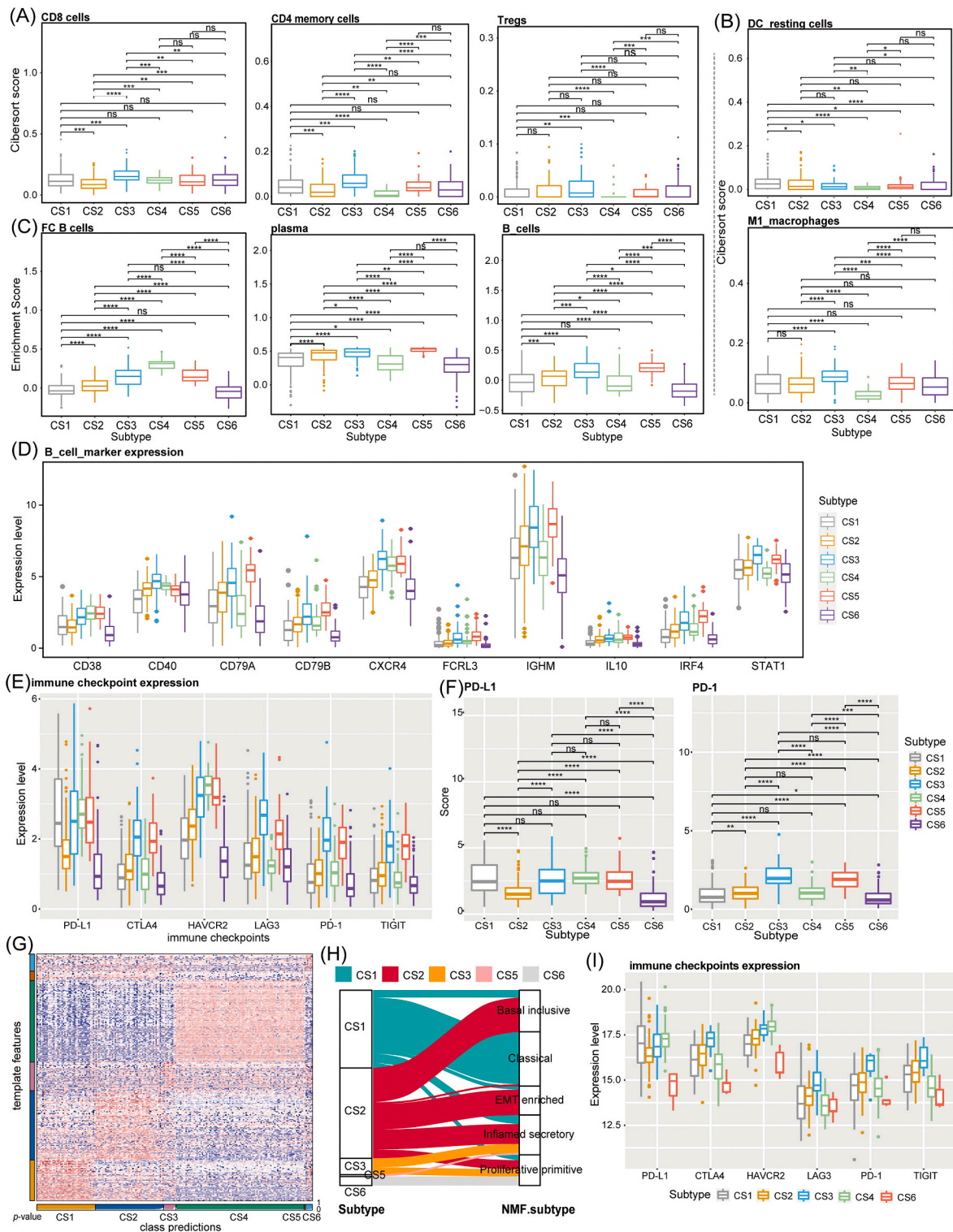
Fig. 2. Scoring and expression of immune signatures in each sub-type. (A, B) Boxplot indicating the immune cell infiltration score of CD8, CD4 memory, Tregs cells (A) and DC_resting, M1_macrophages (B) in each sub-type, which was predicted by the CIBERSORT package. The *P* value was calculated by wilcox.test. ****: P < 0.0001, ***: 0.0001 ≤ P < 0.001, **: 0.001 ≤ P < 0.01, *: 0.01 ≤ P < 0.05, ns: no signature. (C) Boxplot showing the enrichment score of FC (Follicular) B cells, plasma and B cellls of samples in each subtype, which was calculated by the ssGSEA algorithm. The P value was calculated by wilcox.test. ****: P < 0.0001, ***: 0.0001 ≤ P < 0.001, **: 0.001 ≤ P < 0.01, *: 0.01 ≤ P < 0.05. (D) The expression of B cell related marker and TIB genes in each sub-type. (E) The expression of 6 immune checkpoints in each sub-type. (F) The boxplot indicating the

difference expression of PD-1 and PD-L1 in each sub-type. The P value was calculated by wilcox.test. ****: P < 0.0001, ***: 0.0001 ≤ P < 0.001, **: 0.001 ≤ P < 0.01, *: 0.01 ≤ P < 0.05, ns: no signature. (G) Heatmap revealing the RNA characterization of the validate data from the published study based on the predefined feature expression profiling of each sub-type identified in this study and these 202 sample were also divided into six classes. P-value of each sample indicating the potential of predicted sub-type. (H) The alluvial diagrams showing the agreement of predicted sub-type in this study and NMF sub-types in published study of the validate data. (I) The expression of 6 immune checkpoints in each sub-type.

secondary antibody, and TSA signal amplification were performed, and antigen repair was performed six times. Nuclei were stained with DAPI. The specific experimental procedure is described in the manufacturer's instructions. Tissue washing should only use double-distilled water and a freshly prepared wash buffer working solution throughout the experiment. The multispectral tissue imaging system (PerkinElmer Vectra®) was used to implement spectral imaging, and Phenochart 1.0 and QuPath 0.3.2 were used for pathology results analysis.

2.8. Statistical analysis

R software (version 4.2.0) was used to perform all statistical analyses using the two-tailed Wilcoxon rank-sum test, except for the different proteins, which were analyzed using the limma method from the limma package (version 3.53.3), and the distribution difference, which was analyzed using the Fisher test. The Kaplan–Meier approach was used for survival analysis, and subsequent findings were compared using the log-rank test. (*p-value <0.05; **p-value <0.005; ***p-value <0.0005; ****p-value <0.00005).

3. Results

3.1. Classification of the LUSC based on RNA-seq data revealed lymphocyte function-activated tumor subtype

To comprehensively explore the genetic molecular characteristics of LUSC, we re-clustered the 513 LUSC samples from the TCGA database based on all RNA-seq data (including mRNA, lncRNA, and miRNA) (Fig. 1A). All samples were divided into six subtypes (CS1–CS6) based on the consensus matrix by combining multiple algorithms (Fig. 1B and S1A). The difference in the overall survival rate among these subtypes was significant (Fig. S1B). Specifically, the CS4 subtype was present in all normal solid tissue samples with distinct transcriptional characteristics (Fig. 1B).

We further performed functional annotation for each subtype based on the subtype-specific features and observed the activation of the glucuronate metabolic process, neuropeptide receptor, and fatty acid omega-hydroxylase activity in CS1; the interleukin 17 signaling pathway and cell killing in CS2; plasma membrane fusion and amacrine cell differentiation in CS6; and alpha-defensins and glutathione hydrolase activity in CS4 (Fig. S1C). CS3 and CS5 specifically upregulated genes related to the positive regulation of the humoral immune response, adaptive immune response, and B cell receptor signaling pathway (Fig. S1C). GSVA analysis of these six subtypes indicated an immune-deficient state in CS1 and CS6 (Fig. 1C), with the main activation of lymphocyte function in CS3; lymphocyte, complement, and leukocyte functions in CS5; macrophage function in CS2; and almost all immune functions in CS4 (Fig. 1C). The prediction of immune and stromal scores using the EASTMATE algorithm also revealed that CS3 and CS5 obtained significantly higher scores than the other tumor subtypes, whereas minor changes in immunity were observed (Fig. 1D). Further enrichment scoring of immune-related gene sets from the ImmPort database indicated the activation of TNF_Family_Members_Receptors, TNF_Family_Members, Antigen_Processing_and_Presentation, and BCR_Signaling_Pathway in subtypes CS3 and CS5 (Fig. 1E and S1D, E). In contrast, CS3 had more patients with advanced-stage disease than CS5 (Fig. 1F–Table S1).

We identified six well-defined subtypes of TCGA-LUSC samples and found that CS3 acted as the lymphocyte function-activated subtype in many patients with advanced-stage disease.

3.2. CS3 subtype showed a distinct tumor immune microenvironment and was validated by an independent RNA-seq data

To further study the tumor immune environment of these subtypes, we explored their immune signatures. Cell-type Identification By Estimating Relative Subsets Of RNA Transcript (CIBERSORT) was used to predict the immune cell composition for each subtype and suggested that CS3 and CS5 have less neutrophil and dendritic cell activation, whereas CS3 has more CD4 memory-activated cells, CD8, M1 macrophages, and Tregs compared with the other subtypes (Fig. 2A, B, and S2A). For B cells, we scored them for each subtype based on the cell markers from a published study [21] using single sample gene set enrichment analysis (ssGSEA) analysis and found that the B cells were also enriched in CS3 and CS5 subtypes except the germinal center B cells (Fig. 2C and S2B).

Classical immune-active genes and B cell marker examinations in each subtype showed higher expression of CD8A, CXCL10, CXCL9, GZMA, GZMB, INFG, and PRF1, as well as B cell markers CD38, CD79A, CD79B, HLA-DRA, and IGHM in CS3 and CS5 than in other tumor subtypes (Fig. 2D and S2C). Additionally, CS3 showed stronger expression of CXCL10, GZMA, INFG, and the B cell function-related genes CD40 and CXCR4, which are activated in B cells and can induce a specific immune response [48,49], compared with CS5 (Fig. 2D and S2C). Immune signature enrichment analysis also showed increased immune cell infiltration (chemokine 12_score [50]), T cells (T cell_receptor_score), CD8 cells (CD8A), and IGG_cluster responses in CS3 and CS5 cells, suggesting that active immunosurveillance was ongoing in these cells (Fig. S2D). Signatures involved in pro-inflammatory responses (STAT1) and immune checkpoints (ICR_INHIB_score, PD-1, and CTLA4) were more enriched in CS3 than in CS5 (Fig. S2D). The expression of classic immune checkpoints, which are also exhausted markers, was significantly increased in the CS3 and CS5 subtypes, whereas LAG3 and PD-1 were
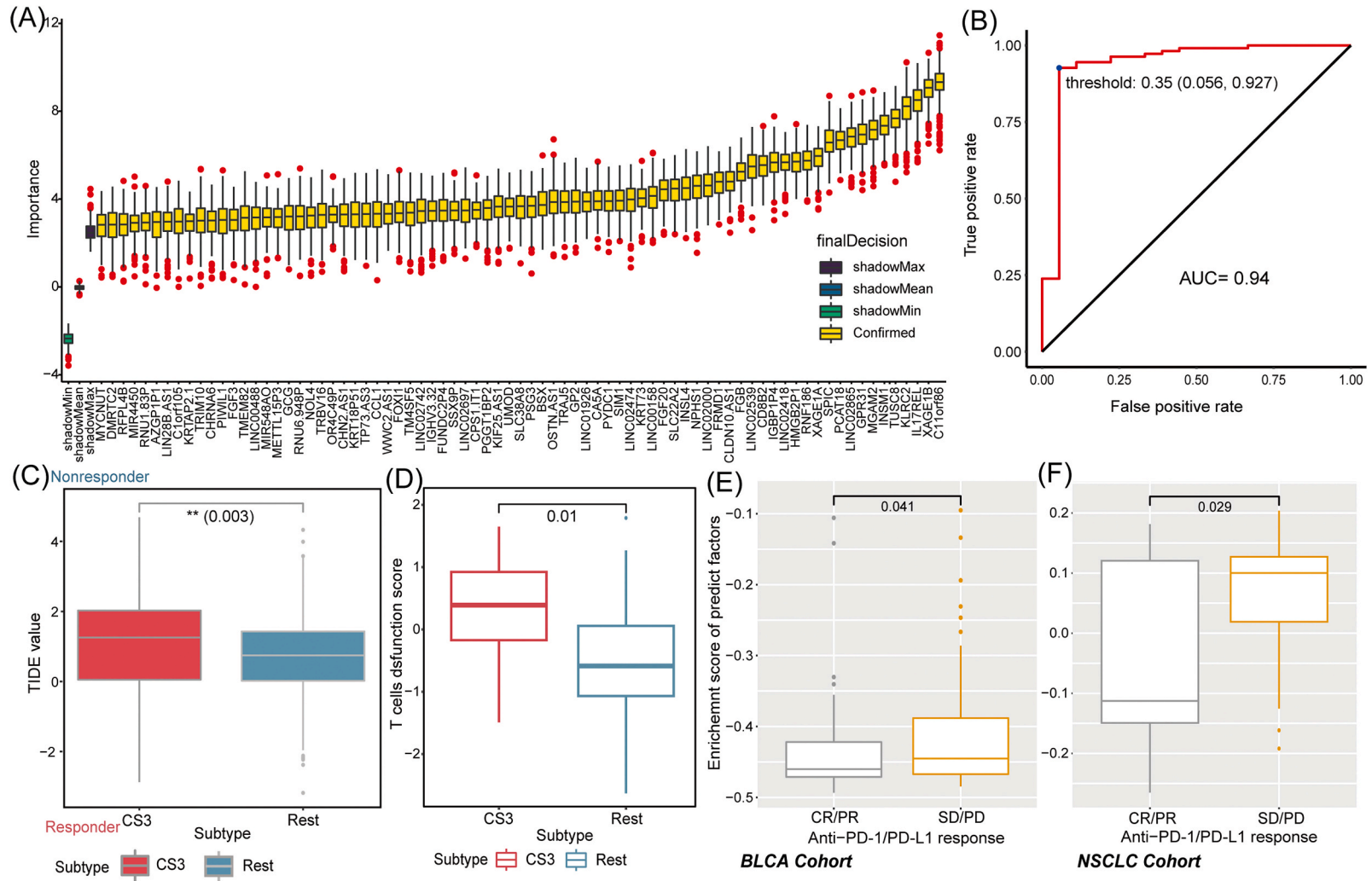
Fig. 3. The identification of predict factors and prediction of response to immunotherapy for CS3 subtype. (A) Boxplot shows the 99 important factors to predict the CS3 sub-type using the boruta algorithm in the 385 train data for random module. (B) ROC curve (receiver operating characteristic curve) showing the sensitivity and specificity in the 128 test data, and calculated the AUC (Area Under Curve) value. (C) Boxplot showing the TIDE (tumour immune dysfunction and exclusion) value of CS3 and Rest sub-type. The P value calculated by the wilcox.test. ****: P < 0.0001, ***: 0.0001 ≤ P < 0.001, **: 0.001 ≤ P < 0.01, *: 0.01 ≤ P < 0.05, ns: no signature. (D) Boxplot showing the T cells dysfunction score by TIDE analysis of CS3 and Rest sub-type in validation data (202 samples). The P value calculated by the wilcox.test. ****: P < 0.0001, ***: 0.0001 ≤ P < 0.001, **: 0.001 ≤ P < 0.01, *: 0.01 ≤ P < 0.05, ns: no signature. (E, F) Boxplot showing the enrichment score of CS3 specific predictive factors in CR/PR and SD/PD groups from the immunotherapy cohort data of urothelial carcinoma (BLCA) (E) and NSCLC (F), which was calculated by ssGSEA analysis. The P value calculated by the wilcox.test. ****: P < 0.0001, ***: 0.0001 ≤ P < 0.001, **: 0.001 ≤ P < 0.01, *: 0.01 ≤ P < 0.05.
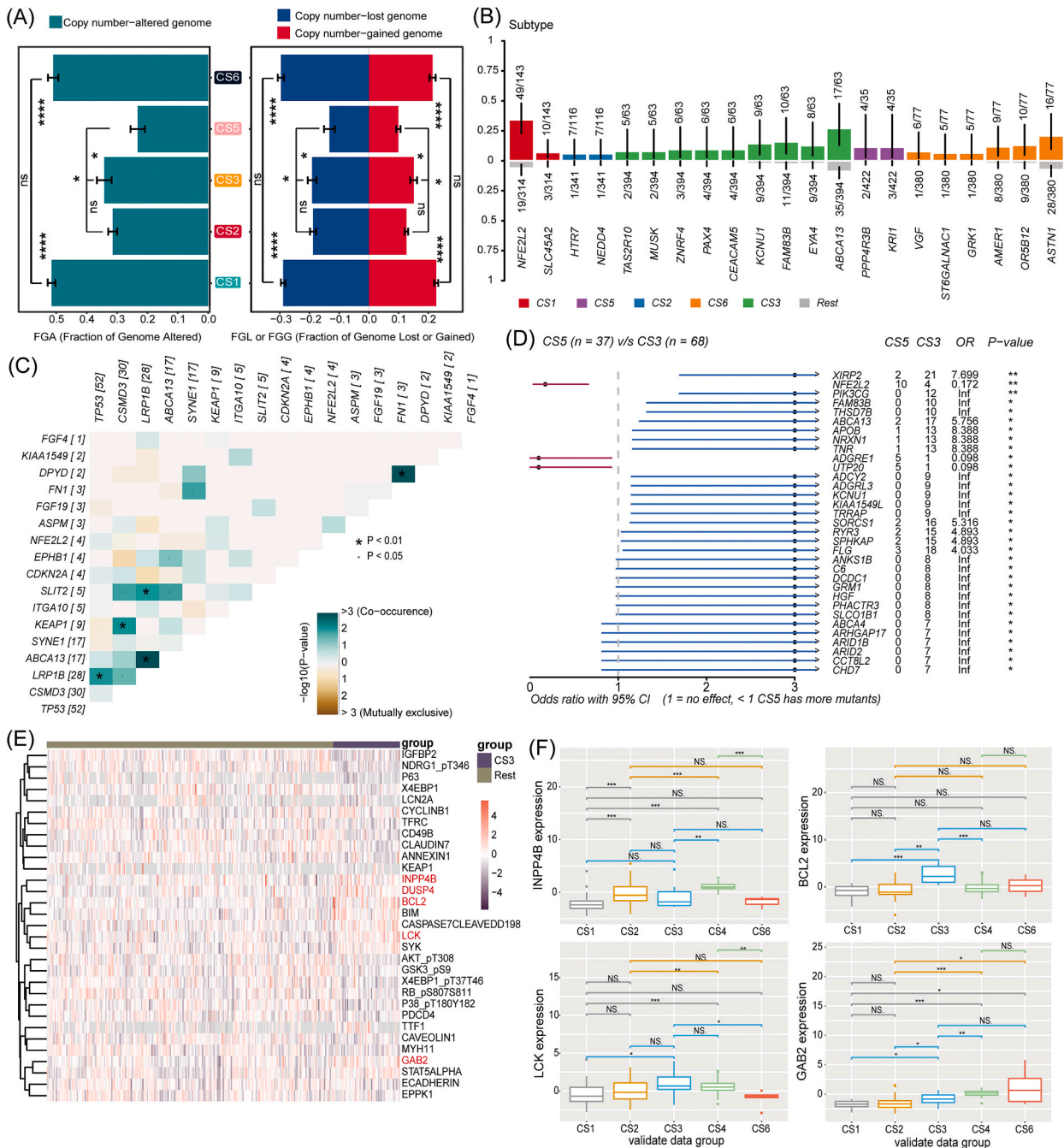
Fig. 4. Molecular characterization of sub-types in LUSC patients. (A) Barplot showing the distribution of FGA (Fraction of Genome Altered), FGL (Fraction of Genome Lost), FGG (Fraction of Genome Gained) and compares them among the six sub-types.The P value was calculated by wilcox.test. ****: P < 0.0001, ***: 0.0001 ≤ P < 0.001, **: 0.001 ≤ P < 0.01, *: 0.01 ≤ P < 0.05, ns: no signature. (B) Somatic interactions analysis revealing the co-occurring or exclusiveness in CS3 subtype based on the selected mutation genes. (C) The distribution of mutation ratio of sub-type specific driver genes compared to the rest sub-types. The P value was calculated by Fisher test. (D) Forestplot shows the gene mutation differences between CS5 versus CS3. OR: odds ratio, CI: confidence interval, ****: P < 0.0001, ***: 0.0001 ≤ P < 0.001, **: 0.001 ≤ P < 0.01, *: 0.01 ≤ P < 0.05, ns: no signature. (E) Heatmap showing the different expressed proteins in CS3 by comparing with the Rest sub-types. The logFoldChange cutoff is 0.25 and FDR cutoff is 0.05. The FDR was the adjusted P value calculated by the limma method. (F) Boxplot showing the protein expression of INPP4B, BCL2, LCK and GAB2 in the predicted sub-types of validate data. ****: P < 0.0001, ***: 0.0001 ≤ P < 0.001, **: 0.001 ≤ P < 0.01, *: 0.01 ≤ P < 0.05, ns: no signature.

highly expressed in CS3 compared to CS5 (Fig. 2E and F).

To further assess the subclustering results, we downloaded the RNA-seq data of 202 LUSC samples (including 108 tumors and 94 adjacent tumors) [39] and reclustered these samples into subclusters with significant p-values using subtype-specific biomarkers (Fig. 2G). The agreement between the predicted subtype and the well-defined classification in the published study revealed that CS3 gathered patients from the inflamed secretory subtype (Fig. 2H). Immune exploration of these predicted subtypes also showed higher immune and stromal scores in CS3, expression of immune-active genes, and immune checkpoints, especially PD-1 (Fig. 2I and S2E–G).

Generally, the CS3 subtype exhibited significant infiltration of lymphocytes, but it also enriched Treg cells and upregulated exhaustion markers, indicating a suppressive role of tumor-infiltrating immune cells in these patients.

3.3. CS3 subtype indicated resistance to ICB therapy by immunotherapy response prediction

To predict the CS3 subtype, we performed random module and Boruta algorithm on bulk RNA-seq-based gene expression profiles of these subtype-specific marker genes and subsequently obtained 99 important genes (Fig. 3A) with an area under the curve of 0.94 in the receiver operating characteristic curve (Fig. 3B). The combined prediction showed that the top 16 genes had the highest accuracy in repeated cross-validation tests (Figs. S3A and B). Among these genes, IL17REL, KLRC2, MGAM2 [51], and XAGE1B [52] are associated with the immune response and immunotherapy, whereas PCAT18, TUSC8, and GPR31 have been reported to be therapeutic targets in tumors [53–55]. Additionally, overall survival analysis of these genes in CS3 patients found that C11orf86 and LINC02539 were significantly correlated with prognosis in patients with the CS3 subtype, whereas IL17REL, KLRC2, INSM1, and XAGE1B were potential prognostic factors (Fig. S3C). Further investigation of the response of patients with CS3 to ICB therapy using the TIDE algorithm [47] revealed that CS3 had higher TIDE prediction scores than the other tumor subtypes (Fig. 3C), and the higher T cells dysfunction score was observed in CS3 from the validation data (Fig. 3D). A higher TIDE prediction score is usually associated with worse ICB response [47]. In the immunotherapeutic cohort of urothelial carcinoma (BLCA) and NSCLC, the significant difference in the enrichment score for CS3-specific predictive factors between the CR/PR and PD/SD groups also revealed that the patients in the CS3 subtype were resistant to ICB therapy (Fig. 3E and F).

3.4. Multiomics molecular characterization of CS3 compared with the other LUSC subtypes revealed the immunosuppressive microenvironment

To systematically examine the multiomics molecular features of the CS3 subtype, we conducted in-depth analyses of its genomic and proteomic profiles. Focusing on the genomic data, we found that the total FGA in CS3 and CS5 was significantly lower than that in the CS1 and CS6 subtypes, whereas the degree of alteration in CS3 was higher than that in CS5 (Fig. 4A). The same change was observed in the fraction of genome lost and the fraction of genome gained (Fig. 4A). Somatic mutation analysis revealed that there was no clear difference in TMB between CS3 and other subtypes, except for CS5 (Figs. S4A and B), and the most frequently mutated gene of CS3-specificity is ATP binding cassette subfamily A member 13 (ABCA13) (27 %) (Fig. 4C, D and S4A), whose expression was mainly associated with drug resistance and malignant progression in various tumors [56]. Comutation detection revealed that ABCA13 usually co-occurred with LRP1B compared with all other tumor subtypes (Fig. 4B and S4C).

Cancer proteomics has revealed key information in mechanistic studies on tumor growth and metastasis, we further performed a difference analysis among these subtypes on protein data and found that INPP4B, dual-specificity phosphatase 4, B cell lymphoma 2 (BCL2), LCK, and GRB2-associated binding protein were specifically increased in CS3 (Fig. 4E and S4D). Among these proteins, INPP4B, a phosphoinositide phosphatase, has been demonstrated to be a tumor suppressor gene. Low expression of INPP4B is associated with poor clinical outcomes [57–60], which also showed decreased expression compared with the normal subtype (CS4) in 202 validation samples (Fig. 4F). Dual-specificity phosphatase 4 has been reported to stabilize the FOXP3 expression in Tregs [61]. Furthermore, BCL2 expression promotes immunosuppression in chronic lymphocytic leukemia, enhancing Tregs differentiation and cytotoxic T cell exhaustion [62]; LCK is an Src family tyrosine kinase essential for T cell development and function and has emerged as a novel druggable target molecule for the treatment of cancer [63,64]; Overexpression of GRB2-associated binding protein can activate immunosuppression of myeloid-derived suppressor cells to accelerate hepatocellular carcinoma progression [65]. All three genes were highly expressed in CS3 compared with other tumor subtypes in the 202 validation samples, especially BCL2 (Fig. 4F).

Thus, multiomics analysis further indicated that the immunosuppressive state of the CS3 subtype, which contains a specific mutated driver gene, ABCA13, overexpressed multiple immunosuppression-related proteins.

3.5. scRNA-seq data analysis uncovered the important role of LAMC2-CD44 for immune resistance in the CS3 subtype

To further investigate the tumor microenvironment and molecular regulation of immune resistance in the CS3 subtype, we predicted the subtype-specific cell composition by combining scRNA-seq data of LUSC from a published study [41] and bulk RNA-seq data from this study using Scissor software (version 2.1.0) [45]. For scRNA-seq data, 42,074 cells from 16 tumor and adjacent tissue samples passed strict quality control and were divided into 37 clusters. These clusters were further annotated as 27 cell types and classified into eight major cell types by classical cell marker genes (Fig. 5A and S5A, B): myeloid cells (CD16$^+$CD68$^+$), CD4_cells (CD4$^+$CD3D+), CD8_cells (CD8A + CD3D+), NK_cells (FGFBP2+GNLY+), plasma cells (JCHAIN + MZB1+), B_cells (MS4A1+CD79A+), Cycle_cells (STMN1+TOP2A+), and non-immune cells. For bulk RNA-seq, we divided the samples into two groups: CS3 and Rest. Scissor analysis predicted 677 CS3-associated cells, mainly B, Plasma, T, and epithelial cells, compared with the cells from the Rest group (Fig. 5B and C).
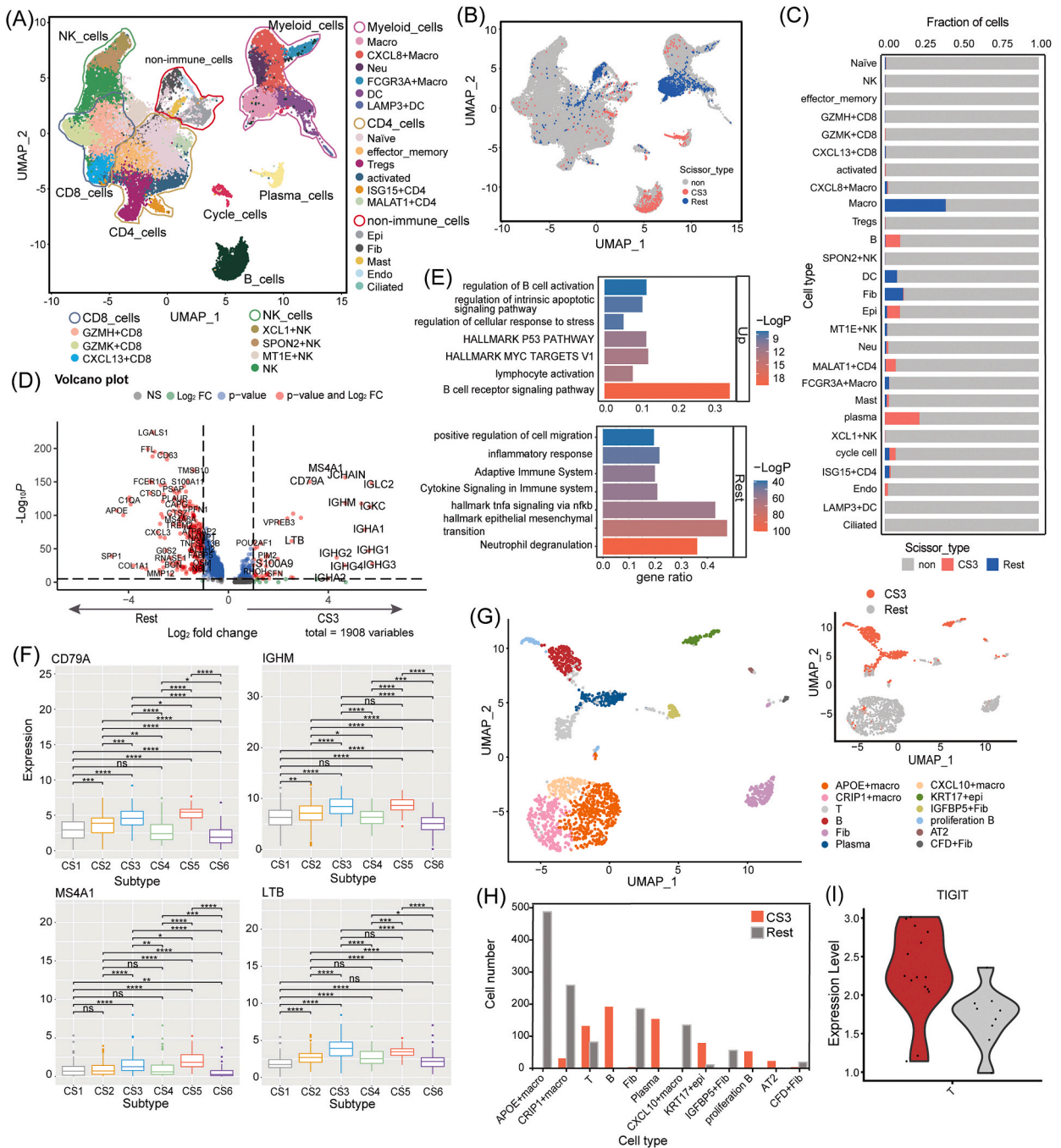
Fig. 5. Lymphocyte enriched sub-type in LUSC patients was validated by the single-cell sequencing data. (A) UMAP visualization of 42,074 cells from 16 LUSC samples in eight main cell types, and the CD8, NK, CD4, Myeloid and non-immune cells further divided into several sub-clusters. (B) UMAP visualization of the Scissor-selected cells. (C) Bar plot shows the distribution of three Scissor cell types across the 27 cell populations. (D) Volcano plot of differential gene expressions in CS3 cells versus Rest cells. The two vertical dashed lines represent $\pm \ln(1.25)$ fold changes, and the horizontal dashed line denotes an FDR cutoff of 0.05. The FDR was the adjusted P value calculated by the two-tailed Wilcoxon rank sum test. (E) Barplot of the enrichment pathways in CS3 cells and Rest cells based on the different genes between them. (F) Boxplot showing the expression of CD79A, IGHM, IGKC and MS4A1 in each identified sub-type in the 202 validation samples. ****: P < 0.0001, ***: 0.0001 ≤ P < 0.001, **: 0.001 ≤ P < 0.01, *: 0.01 ≤ P < 0.05, ns: no signature. (G) UMAP visualization of sub-clustering for the CS3 cells and annotated into 12 sub-clusters. (H) Bar plot shows the distribution of CS3 and Rest cells across the 12 cell populations. (I) The expression of TIGIT in the effector T cells between CS3 and Rest group.
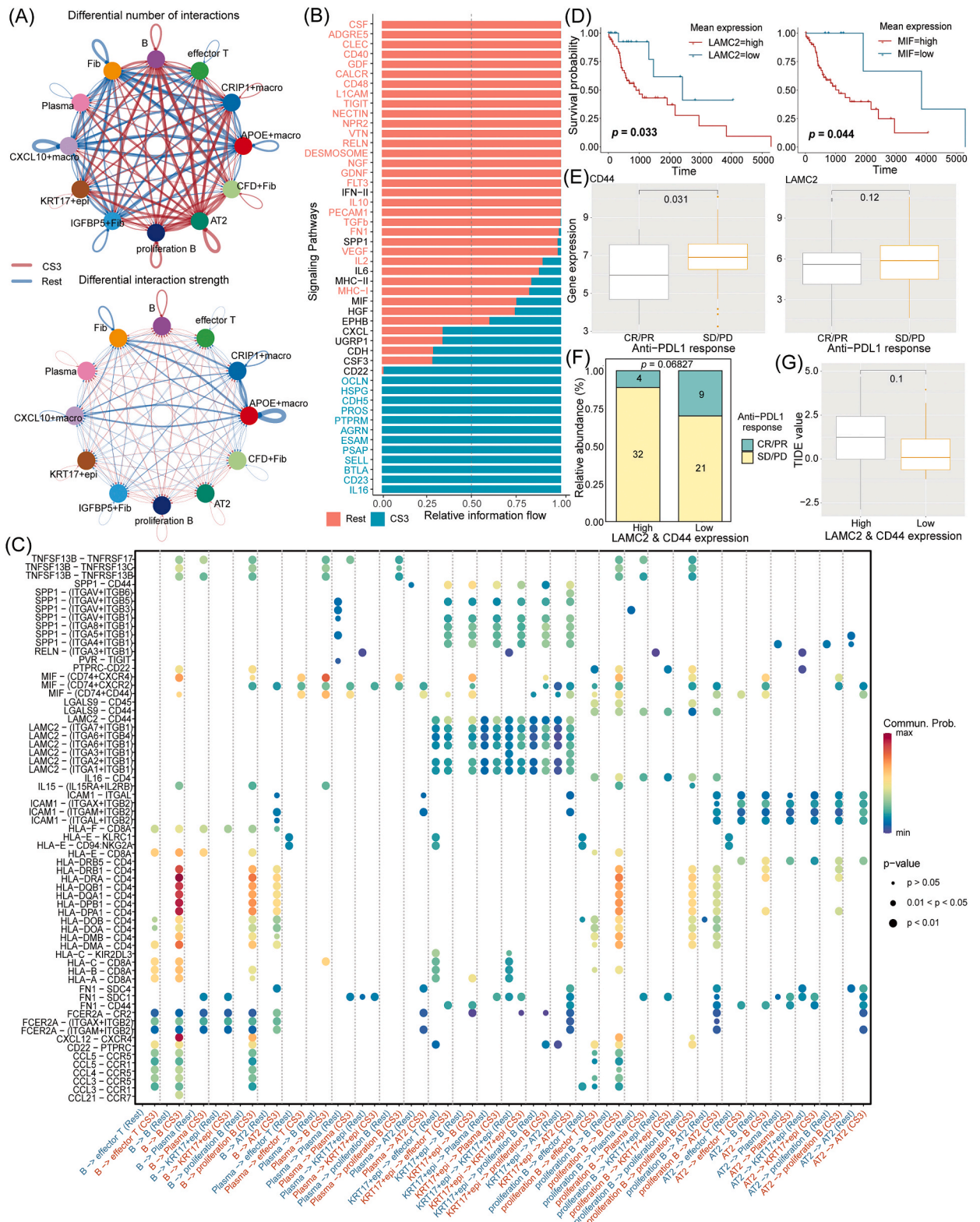
(caption on next page)

Fig. 6. The cell-cell communication and signaling response in CS3 subtype. (A) Network plots showing the differential number and strength of interaction among all cell types from CS3 and Rest groups. The color represented the communication probability. (B) Some selected significant signaling pathways were ranked based on their differences of overall information flow within the inferred networks between CS3 and Rest. The top signaling pathways colored red are more enriched in Rest, the middle ones colored black are equally enriched in CS3 and Rest, and the bottom ones colored green are more enriched in CS3. (C) Some selected significant ligand-receptor pairs that contribute to the signaling sending between cell types from CS3 and Rest. The dot color and size represent the calculated communication probability and p-values. p-values are computed from one-sided permutation test. (D) Overall survival of expression of LAMC2 and LAMC2&CD44 genes in patients from CS3 subtype. Kaplan-Meier survival curves showed the different correlation between OS and expression level of candidate genes. (E) Boxplot showing the expression of CD44 and LAMC2 genes in patients with the high CS3 predictor enrichment score for CR/PR and SD/PD groups from the immunotherapy cohort data of BLCA, which was calculated by ssGSEA analysis. The P value calculated by the wilcox.test. (F) Distribution of the CR/PR and SD/PD patients in LAMC2 & CD44 expression groups and the P value was calculated by Fisher test. (G) Boxplot showing the TIDE value of patients in CS3 subtype for LAMC2 & CD44 expression groups. The P value calculated by the wilcox.test. (For interpretation of the references to color in this figure legend, the reader is referred to the Web version of this article.)

Subsequently, different analyses between the cells from the CS3 and Rest groups showed marked expression of immunoglobulin genes and LTB in the CS3 group (Fig. 5D and S5C). The genes specifically expressed in CS3 were mainly involved in regulating lymphocyte activation, B cell receptor signaling, and hallmark pathways, such as p53 and myc (Fig. 5E). Resting-specific genes participate in cell migration, neutrophil degranulation, EMT, and the adaptive immune system (Fig. 5E). Genes highly expressed in the cells of CS3 were also observed in the bulk RNA-seq data (Fig. 5F). To further analyze the cell composition, we subgrouped the cells of the CS3 and Rest groups and found massive enrichment of B, epithelial, and T cells in CS3 compared with the Rest group (Fig. 5G and H), while the exhausted marker TIGIT had higher expression in T cells from CS3 than in the Rest group (Fig. 5I and S5D).

To better understand the global communication among cells in CS3, we applied cell-cell communication analysis of these cell types and revealed increased interaction among B, plasma, epithelial, and fibroblast cells in the CS3 phenotype compared with the Rest group (Fig. 6A and S6A). Comparison of signaling pathways between the two groups revealed that the IL16, SELL, BTLA, PSAP, AGRN, and PTPRM pathways were specifically activated in CS3, and the IL6, MHC-II, MIF, CXCL, and CSF3 pathways were enriched in both groups (Fig. 6B). For the plasma and proliferation of B cells, the cells from CS3 specifically activated the CXCL, MHC-I, BAFF, and GALECTIN pathways (Fig. S6B).

Compared with the Rest group, the cross-talk among B, Plasma, Proliferation B, T, and epithelial cells activated the MIF, MHC-II, and CXCL pathways in CS3 cells through the molecular communication of MIF-(CD74+CXCR4/CD44), CXCL12-CXCR4, and HLA family factors - CD4/CD8A (Fig. 6C and S6C). Furthermore, we found that epithelial cells could interact with B and T lymphocytes through the communication of SPP1-CD44 and LAMC2-CD44 molecular pairs in the CS3 group (Fig. 6C). Among these molecules, LAMC2 was specifically expressed in KRT17+ epithelial cells, whereas CD44, whose expression is inversely related to T cell infiltration, was expressed in all cells and was highly expressed in cells from the CS3 group (Fig. S6D). High expression of LAMC2 was significantly related to the poor prognosis of patients from the CS3 subtype, and the co-hyperexpression of LAMC2 and CD44 was potentially associated with poor prognosis (Fig. 6D). In addition, a higher expression of CD44/LAMC2 was observed in the PD/SD group than in the CR/PR group (Fig. 6E). The patient group that highly expressed CD44 and LAMC2 had more PD/SD samples and higher TIDE values (Fig. 6F and G).

CS3 is a lymphocyte-infiltrating tumor subtype, and the molecular communication of LAMC2-CD44 plays an important role in immune resistance in the CS3 subtype.

3.6. The expression of LAMC2/CD44 enhances the inhibitory effect of lymphocyte infiltration in the CS3 subtype

We further explored the relationship between the expression of LAMC2/CD44 and immune-related features in the CS3 subtype and found an inverse correlation between LAMC2/CD44 expression and lymphocyte infiltration and a positive correlation between CD44 expression and exhausted markers (Fig. S7A). Specifically, patients with high LAMC2 expression showed lower infiltration scores of CD4_memory_activated, T_follicular_helper, CD8_cells, B_cell_ naïve, and Plasma cells and higher scores of Tregs, as well as higher expression of cancer development- and progression-related genes MMP2, MMP9, and VEGFA (Figs. S7B and C) than patients with low LAMC2 expression. Patients with higher CD44 expression also had lower lymphocyte infiltration scores and higher expression of the exhaustion markers TIGIT, HAVCR2, CTLA4, and MMP2 (Figs. S7D and E). These findings were also observed in the validation dataset (Figs. S7F and G).

3.7. Co-hyperexpression of LAMC2-CD44 contributed to the immune resistance of the CS3 subtype

The above results revealed that the expression of LAMC2/CD44 is inversely related to lymphocyte infiltration and the co-hyperexpression of LAMC2 and CD44 is positively related to immune resistance to ICB therapy in the CS3 subtype, as well as a positive correlation ($R^2 = 0.41$) between LAMC2 and CD44 (Fig. 7A). Thus, we further examined the relationship between the co-expression of LAMC2-CD44 and immune features in the CS3 subtype and found lower infiltration of naïve B, Plasma, CD8, T follicular helper, and NK-activated cells and higher infiltration of Tregs in the co-hyperexpression of LAMC2 and CD44 groups compared with the low expression group (Fig. 7B). We also observed a higher expression of the exhausted markers CTLA4, HAVCR2, LAG3, and TIGIT in the co-hyperexpression group (Fig. 7C). Multicolor immunofluorescent staining further revealed that the co-hyperexpression of LAMC2 and CD44 significantly reduced the infiltration of T and B lymphocytes (Fig. 7D).
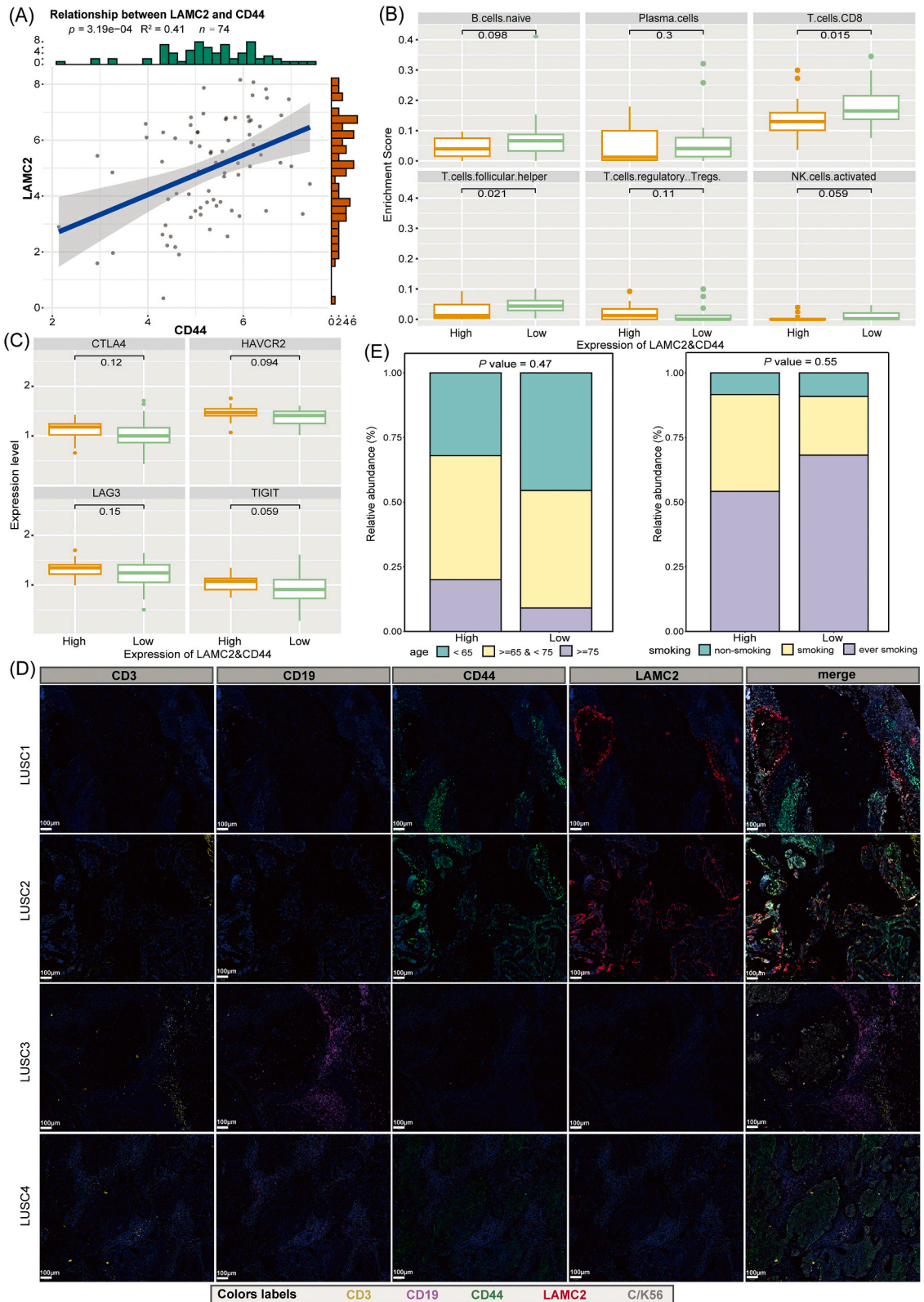
(caption on next page)

Fig. 7. The relationship between the co-expression expression of LAMC2 and CD44 and immune infiltration. (A) The relationship between LAMC2 and CD44 in CS3 subtype based on RNA-seq data. (B) Boxplot showing the Cibersort score of immune cells in the High group of co-expression of LAMC2 and CD44 and Low expression group. The P value was calculated by wilcox.test. ****: P < 0.0001, ***: 0.0001 ≤ P < 0.001, **: 0.001 ≤ P < 0.01, *: 0.01 ≤ P < 0.05, ns: no signature. (C) Boxplot showing the expression of exhausted markers in the High group of co-expression of LAMC2 and CD44 and Low expression group. The P value was calculated by wilcox.test. ****: P < 0.0001, ***: 0.0001 ≤ P < 0.001, **: 0.001 ≤ P < 0.01, *: 0.01 ≤ P < 0.05, ns: no signature. (D) Multicolor IHC staining for verifying the negative relationship between the infiltration of lymphocytes and co-hyperexpression of LAMC2-CD44 in 4 LUSC tissues. The scale bar represents 100 μm. (E) Number distribution of the different age and smoking groups in LAMC2 & CD44 expression groups and the P value was calculated by Fisher test.

We further investigated the expression differences of LAMC2 and CD44 among different clinical phenotype groups and revealed that the expression of LAMC2 showed a partially positive correlation with the age of the patients ($p = 0.08$), whereas there was no clear correlation between CD44 expression and age (Figs. S8A and B). Both groups showed no significant differences in the other clinical phenotypes (Figs. S8A and B). Focusing on the co-expression of LAMC2 and CD44, we observed more older patients ($p = 0.47$) and fewer ever-smoked patients in the high expression group than in the low expression group (Fig. 7E), whereas there was no difference in sex and stage groups (Fig. S8C).

Thus, co-hyperexpression of LAMC2-CD44 contributes to the immunosuppressive microenvironment of the CS3 subtype and is positively related to patient age.

4. Discussion

The advent and breakthroughs in cancer immunotherapy have revolutionized the clinical treatment scheme for LUSC [7,8,66,67]. However, owing to the high heterogeneity of tumors, many patients do not benefit from it. We divided the 513 TCGA-LUSC samples into six subtypes (CS1–CS6) based on RNA-seq data. Immune exploration of these subtypes showed that CS3 is a lymphocyte-infiltrated phenotype, which contains many patients with advanced-stage disease, highly expresses immune-active genes, and shows high expression of immune checkpoints and resistance to ICB therapy. scRNA-seq data analysis also revealed the enrichment of lymphocytes and communication between cancer cells and lymphocytes through LAMC2-CD44 in the CS3 subtype. Further exploration of LAMC2 and CD44 showed that co-hyperexpression of LAMC2-CD44 was negatively correlated with the lymphocyte infiltration score and positively correlated with the Treg infiltration score and the expression of exhausted markers, which were validated using mIHC. LAMC2-CD44 plays an important role in the immune resistance to CS3.

Among the six subtypes, CS3 and CS5 highly expressed immune-active and B cell marker genes, but they also upregulated the immune checkpoints PD-1, CTLA4, and LAG3, which are also markers of exhausted T cells [68,69], and checkpoints are expressed on activated immune cells to prevent overabundance [70]. Furthermore, CS3 contained more patients with advanced-stage disease than CS5, who are more likely to not respond to immunotherapy due to their high heterogeneity. Thus, although CS3 is an immune response-active microenvironment, the infiltrating T lymphocytes play a suppressive role.

Compared with other tumor subtypes, the CS3 subtype showed higher infiltration of B, CD4 memory activated, and CD8 cells, and lower infiltration of DC (Fig. 2A and B) with upregulation of immune-active markers, such as the B cell function-related genes CD40, CXCR4, and STAT1 [48,49]. However, it also enriches Treg cells, which act as immunosuppressive cells by mediating tumor progression and immune escape of cancers [71]. Combined analysis with scRNA-seq data also showed the enrichment of lymphocytes in CS3, but the T lymphocytes from CS3 highly expressed the exhaustion marker TIGIT. These results further reveal the immunosuppressive microenvironment of the CS3 subtype. CS3 enriches many B cells and upregulates IG genes. Multiple studies have indicated that increased tumor B lymphocyte infiltration and IgA B cell production are positively correlated with the efficacy of immunotherapy [72,73]. Thus, targeting B cells may be an effective measure to enhance the immunotherapy response in this subtype.

Multiomics analysis of CS3 revealed a high mutation ratio of the driver gene ABCA13; however, few studies have elucidated the correlation between ABCA13 mutations and the immune response. We also found a high mutation (16 %) in FAM83B, which is reported as a potential therapeutic target in lung adenocarcinoma [74]. Furthermore, multiple immunosuppression-related proteins have been identified in CS3, indicating that these proteins may activate immune responses.

Further exploration of cell-cell communication revealed the protumor microenvironment in the CS3 subtype by molecular communication of MIF/SPP1/LAMC2-CD44 among epithelial, B, and T lymphocyte interactions. Communication between MIF/LAMC2 and CD44 molecular pairs plays tumorigenic roles [75–77], and the SPP1-CD44 pair plays an immunosuppressive role in tumors [77]. Although the difference in the expression of LAMC2 was not significant between the CR/PR and PD/SD groups, the expression of LAMC2 was positively correlated with tumor progression, and the high expression of CD44 resulted in T cell exhaustion. Furthermore, the high expression of both CD44 and LAMC2 resulted in more PD/SD samples, and the co-hyperexpression of LAMC2 and CD44 contributed to lower infiltration of lymphocytes and high expression of exhausted markers. The infiltration of T cells is one step in the cancer-immunity cycle that contributes to varying degrees of immunotherapy resistance [40,78–80]. A previous study also observed high expression of exhausted markers, such as PD-L1 and TIGIT, in the T cells of resistant patients [81]. The expression of inhibitory receptors is associated with tumor progression in patients with NSCLC treated with anti-PD-1 inhibitors and resistance to ICI therapy [82–85]. Thus, the co-hyperexpression of LAMC2-CD44 enhances the exhausted tumor microenvironment of the CS3 subtype, which suggests that the CS3 subtype can potentially improve immunological efficacy by targeting this molecule pair in combination with immunotherapy.

Despite these promising results, we must acknowledge that there are certain limitations. The functions of these molecular pairs require further exploration and validation. In future studies, we will expand the sample size to explore the molecular mechanisms in

advanced patients who do not respond to ICB therapy.

5. Conclusion

In summary, we identified a lymphocyte-infiltrated subtype CS3 for LUSC, which exhibited resistance to ICB therapy with the high expression of multiple immunosuppression-related features and molecular communication of LAMC2-CD44 between epithelial cells and lymphocytes. Targeting this molecule pair in combination with immunotherapy could potentially improve immunological efficacy.

Data availability statement

The data associated with this study been deposited into a publicly available repository. Our study is based on open-source data, so there are no ethical issues and no conflict of interest. Users can download relevant data free for research and publish relevant articles.

Ethics approval and consent to participate

Published data are included in this paper. Ethical approval was obtained from all the patients involved in this study. Users can download relevant data free for research and publish relevant articles. Our study was based on open-source data; therefore, there were no ethical issues or conflicts of interest.

Consent for publication

All the authors consent for publication.

CRediT authorship contribution statement

Tingting Song: Writing – review & editing, Writing – original draft, Visualization, Formal analysis, Data curation. **Ying Yang:** Writing – original draft, Validation, Data curation. **Yilong Wang:** Writing – original draft, Investigation, Data curation. **Yinyun Ni:** Writing – original draft, Data curation. **Yongfeng Yang:** Writing – review & editing, Writing – original draft, Funding acquisition, Conceptualization. **Li Zhang:** Writing – review & editing, Writing – original draft, Funding acquisition, Conceptualization.

Declaration of competing interest

The authors declare that they have no known competing financial interests or personal relationships that could have appeared to influence the work reported in this paper.

Appendix A. Supplementary data

Supplementary data to this article can be found online at https://doi.org/10.1016/j.heliyon.2024.e31299.

References

[1] J.A. Barta, C.A. Powell, J.P. Wisnivesky, Global epidemiology of lung cancer, Ann Glob Health 85 (1) (2019) 8, https://doi.org/10.5334/aogh.2419.
[2] R.L. Siegel, K.D. Miller, N.S. Wagle, A. Jemal, Cancer statistics, 2023, CA Cancer J Clin 73 (1) (2023) 17–48, https://doi.org/10.3322/caac.21763.

[3] Cancer Genome Atlas Research Network, Comprehensive genomic characterization of squamous cell lung cancers, Nature 489 (7417) (2012) 519–525, https://doi.org/10.1038/nature11404.

[4] P.K. Paik, R.N. Pillai, C.S. Lathan, S.A. Velasco, V. Papadimitrakopoulou, New treatment options in advanced squamous cell lung cancer, Am Soc Clin Oncol Educ Book 39 (2019) e198–e206, https://doi.org/10.1200/EDBK_237829.

[5] R.S. Heist, L.V. Sequist, J.A. Engelman, Genetic changes in squamous cell lung cancer: a review, J. Thorac. Oncol. 7 (5) (2012) 924–933, https://doi.org/10.1097/JTO.0b013e31824cc334.

[6] H. Parvaresh, G. Roozitalab, F. Golandam, P. Behzadi, P. Jabbarzadeh Kaboli, Unraveling the potential of ALK-targeted therapies in non-small cell lung cancer: comprehensive insights and future directions, Biomedicines 12 (2) (2024) 297, https://doi.org/10.3390/biomedicines12020297.

[7] N. Karachaliou, M. Fernandez-Bruno, R. Rosell, Strategies for first-line immunotherapy in squamous cell lung cancer: are combinations a game changer? Transl. Lung Cancer Res. 7 (Suppl 3) (2018) S198–S201, https://doi.org/10.21037/tlcr.2018.07.02.

[8] L. Paz-Ares, A. Luft, D. Vicente, et al., Pembrolizumab plus chemotherapy for squamous non-small-cell lung cancer, N. Engl. J. Med. 379 (21) (2018) 2040–2051, https://doi.org/10.1056/NEJMoa1810865.

[9] E. Felip, N. Altorki, C. Zhou, et al., Adjuvant atezolizumab after adjuvant chemotherapy in resected stage IB-IIIA non-small-cell lung cancer (IMpower010): a randomised, multicentre, open-label, phase 3 trial, Lancet 398 (10308) (2021) 1344–1357, https://doi.org/10.1016/S0140-6736(21)02098-5.

[10] P.M. Forde, J. Spicer, S. Lu, et al., Neoadjuvant nivolumab plus chemotherapy in resectable lung cancer, N. Engl. J. Med. 386 (21) (2022) 1973–1985, https://doi.org/10.1056/NEJMoa2202170.

[11] B.A. Derman, K.F. Mileham, P.D. Bonomi, M. Batus, M.J. Fidler, Treatment of advanced squamous cell carcinoma of the lung: a review, Transl. Lung Cancer Res. 4 (5) (2015) 524–532, https://doi.org/10.3978/j.issn.2218-6751.2015.06.07.

[12] W.H. Fridman, F. Pagès, C. Sautès-Fridman, J. Galon, The immune contexture in human tumours: impact on clinical outcome, Nat. Rev. Cancer 12 (4) (2012) 298–306, https://doi.org/10.5334/aogh.2419.

[13] W.H. Fridman, L. Zitvogel, C. Sautès-Fridman, G. Kroemer, The immune contexture in cancer prognosis and treatment, Nat. Rev. Clin. Oncol. 14 (12) (2017) 717–734, https://doi.org/10.1038/nrclinonc.2017.101.

[14] F. Pagès, B. Mlecnik, F. Marliot, et al., International validation of the consensus Immunoscore for the classification of colon cancer: a prognostic and accuracy study, Lancet 391 (10135) (2018) 2128–2139, https://doi.org/10.1016/S0140-6736(18)30789-X.

[15] B.L. Horton, D.M. Morgan, N. Momin, et al., Lack of CD8+ T cell effector differentiation during priming mediates checkpoint blockade resistance in non-small cell lung cancer, Sci Immunol 6 (64) (2021) eabi8800, https://doi.org/10.1126/sciimmunol.abi8800.

[16] G. Morad, B.A. Helmink, P. Sharma, J.A. Wargo, Hallmarks of response, resistance, and toxicity to immune checkpoint blockade, Cell 184 (21) (2021) 5309–5337, https://doi.org/10.1016/j.cell.2021.09.020.

[17] C. Germain, S. Gnjatic, F. Tamzalit, et al., Presence of B cells in tertiary lymphoid structures is associated with protective immunity in patients with lung cancer, Am. J. Respir. Crit. Care Med. 189 (7) (2014) 832–844, https://doi.org/10.1164/rccm.201309-1611OC.

[18] A. Mantovani, P. Allavena, F. Marchesi, C. Garlanda, Macrophages as tools and targets in cancer therapy, Nat. Rev. Drug Discov. 21 (11) (2022) 799–820, https://doi.org/10.1038/s41573-022-00520-5.

[19] S. Inoue, W.W. Leitner, B. Golding, et al., Inhibitory effects of B cells on antitumor immunity, Cancer Res. 66 (15) (2006) 7741–7747, https://doi.org/10.1158/0008-5472.CAN-05-3766.

[20] C.M. Laumont, A.C. Banville, M. Gilardi, D.P. Hollern, B.H. Nelson, Tumour-infiltrating B cells: immunological mechanisms, clinical impact and therapeutic opportunities, Nat. Rev. Cancer 22 (7) (2022) 414–430, https://doi.org/10.1038/s41568-022-00466-1.

[21] N.S. Patil, B.Y. Nabet, S. Müller, et al., Intratumoral plasma cells predict outcomes to PD-L1 blockade in non-small cell lung cancer, Cancer Cell 40 (3) (2022) 289–300.e4, https://doi.org/10.1016/j.ccell.2022.02.002.

[22] Y.Q. Ao, J. Gao, L.X. Zhang, et al., Tumor-infiltrating CD36+CD8+T cells determine exhausted tumor microenvironment and correlate with inferior response to chemotherapy in non-small cell lung cancer, BMC Cancer 23 (1) (2023) 367, https://doi.org/10.1186/s12885-023-10836-z.

[23] S.S. Wang, W. Liu, D. Ly, H. Xu, L. Qu, L. Zhang, Tumor-infiltrating B cells: their role and application in anti-tumor immunity in lung cancer, Cell. Mol. Immunol. 16 (1) (2019) 6–18, https://doi.org/10.1038/s41423-018-0027-x.

[24] D.G. DeNardo, B. Ruffell, Macrophages as regulators of tumour immunity and immunotherapy, Nat Rev Immuno 19 (6) (2019) 369–382, https://doi.org/10.1038/s41577-019-0127-6.

[25] I.S. Kim, Y. Gao, T. Welte, et al., Immuno-subtyping of breast cancer reveals distinct myeloid cell profiles and immunotherapy resistance mechanisms, Nat. Cell Biol. 21 (9) (2019) 1113–1126, https://doi.org/10.1038/s41556-019-0373-7.

[26] P.D.A. Vignali, K. DePeaux, M.J. Watson, et al., Hypoxia drives CD39-dependent suppressor function in exhausted T cells to limit antitumor immunity, Nat. Immunol. 24 (2) (2023) 267–279, https://doi.org/10.1038/s41590-022-01379-9.

[27] J.A. Belk, B. Daniel, A.T. Satpathy, Epigenetic regulation of T cell exhaustion, Nat. Immunol. 23 (6) (2022) 848–860, https://doi.org/10.1038/s41590-022-01224-z.

[28] N. Weisshaar, J. Wu, Y. Ming, et al., Rgs16 promotes antitumor CD8+ T cell exhaustion, Sci Immunol 7 (71) (2022) eabh1873, https://doi.org/10.1126/sciimmunol.abh1873.

[29] P. Behzadi, A.S. Sameer, S. Nissar, et al., The interleukin-1 (IL-1) superfamily cytokines and their single nucleotide polymorphisms (SNPs), J Immunol Res 2022 (2022) 2054431, https://doi.org/10.1155/2022/2054431.

[30] S. Mukherjee, R. Patra, P. Behzadi, A. Masotti, A. Paolini, M. Sarshar, Toll-like receptor-guided therapeutic intervention of human cancers: molecular and immunological perspectives, Front. Immunol. 14 (2023) 1244345, https://doi.org/10.3389/fimmu.2023.1244345.

[31] H. Xu, M. Niu, X. Yuan, K. Wu, A. Liu, CD44 as a tumor biomarker and therapeutic target, Exp. Hematol. Oncol. 9 (1) (2020) 36, https://doi.org/10.1186/s40164-020-00192-0.

[32] A. Sadeghi, R. Roudi, A. Mirzaei, A. Zare Mirzaei, Z. Madjd, M. Abolhasani, CD44 epithelial isoform inversely associates with invasive characteristics of colorectal cancer, Biomark Med 13 (6) (2019) 419–426, https://doi.org/10.2217/bmm-2018-0337.

[33] Y.W. Moon, G. Rao, J.J. Kim, et al., LAMC2 enhances the metastatic potential of lung adenocarcinoma, Cell Death Differ. 22 (8) (2015) 1341–1352, https://doi.org/10.1038/cdd.2014.228.

[34] M. Liu, R. Cai, T. Wang, et al., LAMC2 promotes the proliferation of cancer cells and induce infiltration of macrophages in non-small cell lung cancer, Ann. Transl. Med. 9 (17) (2021) 1392, https://doi.org/10.21037/atm-21-4507.

[35] D. Grün, A. van Oudenaarden, Design and analysis of single-cell sequencing experiments, Cell 163 (4) (2015) 799–810, https://doi.org/10.1016/j.cell.2015.10.039.

[36] J.M. Taube, G. Akturk, M. Angelo, et al., The Society for Immunotherapy of Cancer statement on best practices for multiplex immunohistochemistry (IHC) and immunofluorescence (IF) staining and validation, J Immunother Cancer 8 (1) (2020) e000155, https://doi.org/10.1136/jitc-2019-000155 [published correction appears in J Immunother Cancer. 2020 Jun;8(1):].

[37] W.C.C. Tan, S.N. Nerurkar, H.Y. Cai, et al., Overview of multiplex immunohistochemistry/immunofluorescence techniques in the era of cancer immunotherapy, Cancer Commun. 40 (4) (2020) 135–153, https://doi.org/10.1002/cac2.12023.

[38] Zhang W, Song ZJ, Zhang BY, et al. Multiplex immunohistochemistry indicates biomarkers in colorectal cancer. Neoplasma 202168(6): 1272-1282. https://doi.org/10.4149/neo_2021_210312N324..

[39] S. Satpathy, K. Krug, P.M. Jean Beltran, et al., A proteogenomic portrait of lung squamous cell carcinoma, Cell 184 (16) (2021) 4348–4371.e40, https://doi.org/10.1016/j.cell.2021.07.016.

[40] S. Mariathasan, S.J. Turley, D. Nickles, et al., TGFβ attenuates tumour response to PD-L1 blockade by contributing to exclusion of T cells, Nature 554 (7693) (2018) 544–548, https://doi.org/10.1038/nature25501.

[41] C. Wang, Q. Yu, T. Song, et al., The heterogeneous immune landscape between lung adenocarcinoma and squamous carcinoma revealed by single-cell RNA sequencing, Signal Transduct Target Ther 7 (1) (2022) 289, https://doi.org/10.1038/s41392-022-01130-8.

[42] X. Lu, J. Meng, Y. Zhou, L. Jiang, F. Yan, MOVICS: an R package for multi-omics integration and visualization in cancer subtyping, Bioinformatics (2020), https://doi.org/10.1093/bioinformatics/btaa1018 btaa1018.

[43] G. Sturm, F. Finotello, F. Petitprez, et al., Comprehensive evaluation of transcriptome-based cell-type quantification methods for immuno-oncology, Bioinformatics 35 (14) (2019) i436–i445, https://doi.org/10.1093/bioinformatics/btz363.

[44] K. Yoshihara, M. Shahmoradgoli, E. Martínez, et al., Inferring tumour purity and stromal and immune cell admixture from expression data, Nat. Commun. 4 (2013) 2612, https://doi.org/10.1038/ncomms3612.

[45] D. Sun, X. Guan, A.E. Moran, et al., Identifying phenotype-associated subpopulations by integrating bulk and single-cell sequencing data, Nat. Biotechnol. 40 (4) (2022) 527–538, https://doi.org/10.1038/s41587-021-01091-3.

[46] P. Behzadi, R. Ranjbar, DNA microarray technology and bioinformatic web services, Acta Microbiol. Immunol. Hung. 66 (1) (2019) 19–30, https://doi.org/10.1556/030.65.2018.028.

[47] P. Jiang, S. Gu, D. Pan, et al., Signatures of T cell dysfunction and exclusion predict cancer immunotherapy response, Nat Med 24 (10) (2018) 1550–1558, https://doi.org/10.1038/s41591-018-0136-1.

[48] K. Wennhold, A. Shimabukuro-Vornhagen, S. Theurich, M. von Bergwelt-Baildon, CD40-activated B cells as antigen-presenting cells: the final sprint toward clinical application, Expert Rev. Vaccines 12 (6) (2013) 631–637, https://doi.org/10.1586/erv.13.39.

[49] J.W. Jang, P.X. Thuy, J.W. Lee, E.Y. Moon, CXCR4 promotes B cell viability by the cooperation of nuclear factor (erythroid-derived 2)-like 2 and hypoxia-inducible factor-1α under hypoxic conditions, Cell Death Dis. 12 (4) (2021) 330, https://doi.org/10.1038/s41419-021-03615-w.

[50] X. Li, Z. Wan, X. Liu, K. Ou, L. Yang, A 12-chemokine gene signature is associated with the enhanced immunogram scores and is relevant for precision immunotherapy, Med. Oncol. 39 (4) (2022) 43, https://doi.org/10.1007/s12032-021-01635-2.

[51] S. Xu, Y. Feng, S. Zhao, Proteins with evolutionarily hypervariable domains are associated with immune response and better survival of basal-like breast cancer patients, Comput. Struct. Biotechnol. J. 17 (2019) 430–440, https://doi.org/10.1016/j.csbj.2019.03.008.

[52] Y. Ohue, S. Eikawa, N. Okazaki, et al., Spontaneous antibody, and CD4 and CD8 T-cell responses against XAGE-1b (GAGED2a) in non-small cell lung cancer patients, Int. J. Cancer 131 (5) (2012) E649–E658, https://doi.org/10.1002/ijc.27359.

[53] N. Shi, D. Feng, Y. Gu, C. Zheng, M. Miao, TUSC8 enhances cisplatin sensitivity of NSCLC cells through regulating VEGFA, J BUON 26 (2) (2021) 336–344.

[54] L. He, J. Wang, L. Zhou, X. Li, LncRNA PCAT18 promotes non-small cell lung cancer progression by sponging miR-4319, Cancer Manag. Res. 13 (2021) 3761–3774, https://doi.org/10.2147/CMAR.S298918.

[55] N. Fehrenbacher, M.R. Philips, Targeting RAS - will GPR31 deliver us a new path forward? Mol Cell Oncol 4 (6) (2017) e1359228 https://doi.org/10.1080/23723556.2017.1359228.

[56] M. Pasello, A.M. Giudice, K. Scotlandi, The ABC subfamily A transporters: Multifaceted players with incipient potentialities in cancer, Semin. Cancer Biol. 60 (2020) 57–71, https://doi.org/10.1016/j.semcancer.2019.10.004.

[57] Y. Chen, Z. Sun, M. Qi, et al., INPP4B restrains cell proliferation and metastasis via regulation of the PI3K/AKT/SGK pathway, J. Cell Mol. Med. 22 (5) (2018) 2935–2943, https://doi.org/10.1111/jcmm.13595.

[58] S.J. Rodgers, L.M. Ooms, V.M.J. Oorschot, et al., INPP4B promotes PI3Kα-dependent late endosome formation and Wnt/β-catenin signaling in breast cancer, Nat. Commun. 12 (1) (2021) 3140, https://doi.org/10.1038/s41467-021-23241-6.

[59] C. Gewinner, Z.C. Wang, A. Richardson, et al., Evidence that inositol polyphosphate 4-phosphatase type II is a tumor suppressor that inhibits PI3K signaling, Cancer Cell 16 (2) (2009) 115–125, https://doi.org/10.1016/j.ccr.2009.06.006.

[60] W. Tang, L. Yang, T. Yang, et al., INPP4B inhibits cell proliferation, invasion and chemoresistance in human hepatocellular carcinoma, OncoTargets Ther. 12 (2019) 3491–3507, https://doi.org/10.2147/OTT.S196832.

[61] D. Yan, J. Farache, M. Mingueneau, D. Mathis, C. Benoist, Imbalanced signal transduction in regulatory T cells expressing the transcription factor FoxP3, Proc Natl Acad Sci U S A 112 (48) (2015) 14942–14947, https://doi.org/10.1073/pnas.1520393112.

[62] L. Liu, X. Cheng, H. Yang, et al., BCL-2 expression promotes immunosuppression in chronic lymphocytic leukemia by enhancing regulatory T cell differentiation and cytotoxic T cell exhaustion, Mol. Cancer 21 (1) (2022) 59, https://doi.org/10.1186/s12943-022-01516-w.

[63] U. Bommhardt, B. Schraven, L. Simeoni, Beyond TCR Signaling: Emerging Functions of Lck in Cancer and Immunotherapy, Int. J. Mol. Sci. 20 (14) (2019) 3500, https://doi.org/10.3390/ijms20143500.

[64] J. Weiße, J. Rosemann, L. Müller, et al., Identification of lymphocyte cell-specific protein-tyrosine kinase (LCK) as a driver for invasion and migration of oral cancer by tumor heterogeneity exploitation, Mol. Cancer 20 (1) (2021) 88, https://doi.org/10.1186/s12943-021-01384-w.

[65] S. Chen, J. Cheng, Y. Zhong, R. Liu, Z. Lu, X. Luo, Liver-specific overexpression of Gab2 accelerates hepatocellular carcinoma progression by activating immunosuppression of myeloid-derived suppressor cells, Oncogene 41 (24) (2022) 3316–3327, https://doi.org/10.1038/s41388-022-02298-7.

[66] D.B. Doroshow, M.F. Sanmamed, K. Hastings, et al., Immunotherapy in Non-Small Cell Lung Cancer: Facts and Hopes, Clin. Cancer Res. 25 (15) (2019) 4592–4602, https://doi.org/10.1158/1078-0432.CCR-18-1538.

[67] S.C.M. Lau, Y. Pan, V. Velcheti, K.K. Wong, Squamous cell lung cancer: Current landscape and future therapeutic options, Cancer Cell 40 (11) (2022) 1279–1293, https://doi.org/10.1016/j.ccell.2022.09.018.

[68] E.J. Wherry, M. Kurachi, Molecular and cellular insights into T cell exhaustion, Nat. Rev. Immunol. 15 (8) (2015) 486–499, https://doi.org/10.1038/nri3862.

[69] X. Guo, Y. Zhang, L. Zheng, et al., Global characterization of T cells in non-small-cell lung cancer by single-cell sequencing, Nat Med 24 (7) (2018) 978–985, https://doi.org/10.1038/s41591-018-0045-3.

[70] P. Jain, C. Jain, V. Velcheti, Role of immune-checkpoint inhibitors in lung cancer, Ther. Adv. Respir. Dis. 12 (2018) 1753465817750075, https://doi.org/10.1177/1753465817750075.

[71] Y. Tie, F. Tang, Y.Q. Wei, X.W. Wei, Immunosuppressive cells in cancer: mechanisms and potential therapeutic targets, J. Hematol. Oncol. 15 (1) (2022) 61, https://doi.org/10.1186/s13045-022-01282-8.

[72] F. Petitprez, A. de Reyniès, E.Z. Keung, et al., B cells are associated with survival and immunotherapy response in sarcoma, Nature 577 (7791) (2020) 556–560, https://doi.org/10.1038/s41586-019-1906-8.

[73] S. Biswas, G. Mandal, K.K. Payne, et al., IgA transcytosis and antigen recognition govern ovarian cancer immunity, Nature 591 (7850) (2021) 464–470, https://doi.org/10.1038/s41586-020-03144-0.

[74] J. Zhang, J. Wang, K. Yue, et al., FAM83B promotes the invasion of primary lung adenocarcinoma via PI3K/AKT/NF-κB pathway, BMC Pulm. Med. 23 (1) (2023) 32, https://doi.org/10.1186/s12890-022-02303-5.

[75] J.C. Penticuff, B.L. Woolbright, T.M. Sielecki, S.J. Weir, J.A. Taylor, MIF family proteins in genitourinary cancer: tumorigenic roles and therapeutic potential, Nat. Rev. Urol. 16 (5) (2019) 318–328, https://doi.org/10.1038/s41585-019-0171-9.

[76] H. Sato, S. Higashi, K. Miyazaki, Amino-terminal fragments of laminin γ2 chain stimulate migration of metastatic breast cancer cells by interacting with CD44, Clin. Exp. Metastasis 32 (5) (2015) 405–415, https://doi.org/10.1007/s10585-015-9705-6.

[77] M. Cheng, G. Liang, Z. Yin, X. Lin, Q. Sun, Y. Liu, Immunosuppressive role of SPP1-CD44 in the tumor microenvironment of intrahepatic cholangiocarcinoma assessed by single-cell RNA sequencing, J. Cancer Res. Clin. Oncol. 149 (9) (2022) 5497–5512, https://doi.org/10.1007/s00432-022-04498-w.

[78] D.S. Chen, I. Mellman, Oncology meets immunology: The cancer-immunity cycle, Immunity 39 (1) (2013) 1–10, https://doi.org/10.1016/j.immuni.2013.07.012.

[79] T. Wu, Y. Dai, Tumor microenvironment and therapeutic response, Cancer Lett. 387 (2017) 61–68, https://doi.org/10.1016/j.canlet.2016.01.043.

[80] S.T. Paijens, A. Vledder, M. de Bruyn, et al., Tumor-infiltrating lymphocytes in the immunotherapy era, Cell. Mol. Immunol. 18 (4) (2021) 842–859, https://doi.org/10.1038/s41423-020-00565-9.

[81] S. Hiltbrunner, L. Cords, S. Kasser, et al., Acquired resistance to anti-PD1 therapy in patients with NSCLC associates with immunosuppressive T cell phenotype, Nat. Commun. 14 (1) (2023) 5154, https://doi.org/10.1038/s41467-023-40745-5.

[82] J. Fu, A. Yu, X. Xiao, et al., CD4+ T cell exhaustion leads to adoptive transfer therapy failure which can be prevented by immune checkpoint blockade, Am. J. Cancer Res. 10 (12) (2020) 4234–4250.

[83] S. Koyama, E.A. Akbay, Y.Y. Li, et al., Adaptive resistance to therapeutic PD-1 blockade is associated with upregulation of alternative immune checkpoints, Nat. Commun. 7 (2016) 10501, https://doi.org/10.1038/ncomms10501.

[84] D.S. Thommen, J. Schreiner, P. Müller, et al., Progression of Lung Cancer Is Associated with Increased Dysfunction of T Cells Defined by Coexpression of Multiple Inhibitory Receptors, Cancer Immunol. Res. 3 (12) (2015) 1344–1355, https://doi.org/10.1158/2326-6066.CIR-15-0097.

[85] S. Kurtulus, K. Sakuishi, S.F. Ngiow, et al., TIGIT predominantly regulates the immune response via regulatory T cells, J. Clin. Invest. 125 (11) (2015) 4053–4062, https://doi.org/10.1172/JCI81187.